New BIOTECHNOLOGY 66 (2022) 36–45

Contents lists available at ScienceDirect

New BIOTECHNOLOGY

journal homepage: www.elsevier.com/locate/nbt

Full length Article

SARS-CoV2 neutralizing activity of ozone on porous and non-porous materials

Stella Wolfgruber [a], Martina Loibner [a], Markus Puff [b], Alexander Melischnig [b], Kurt Zatloukal [c,*]

[a] Diagnostic- and Research Center for Molecular Biomedicine, Institute of Pathology, Medical University of Graz, Graz, Austria
[b] TDK Electronics GmbH & Co OG, Deutschlandsberg, Austria
[c] Diagnostic- and Research Center for Molecular Biomedicine, Institute of Pathology, Medical University of Graz, Graz, Austria

ARTICLE INFO

Keywords:
FFP3 mask
Cotton mask
Disinfection
Ozone
SARS-CoV-2
Cold plasma

ABSTRACT

The COVID-19 pandemic has generated a major need for non-destructive and environmentally friendly disinfection methods. This work presents the development and testing of a disinfection process based on gaseous ozone for SARS-CoV-2-contaminated porous and non-porous surfaces. A newly developed disinfection chamber was used, equipped with a CeraPlas™ cold plasma generator that produces ozone during plasma ignition. A reduction of more than log 6 of infectious virus could be demonstrated for virus-contaminated cotton and FFP3 face masks as well as glass slides after exposure to 800 ppm ozone for 10−60 min, depending on the material. In contrast to other disinfectants, ozone can be produced quickly and cost-effectively, and its environmentally friendly breakdown product oxygen does not leave harmful residues. Disinfection with ozone could help to overcome delivery difficulties of personal protective equipment by enabling safe reuse with further applications, thereby reducing waste generation, and may allow regular disinfection of personal items with non-porous surfaces.

Introduction

SARS-CoV-2, the causative coronavirus agent of the infectious disease COVID-19, is mainly transmitted via respiratory droplets and aerosols. Direct contact with virus-contaminated surfaces such as cell phones, computer keyboards or door handles can also lead to infections, and fecal-oral transmission has been reported [1–4]. The survival time of SARS-CoV-2 on various surfaces has been described [5], with recovery of infectious virus for up to 28 days when dried on non-porous surfaces such as glass or metal at 20 °C and 50 % relative humidity. Another study recovered SARS-CoV-2 from plastic surfaces for up to 28 days at room temperature (RT) and 40–50 % relative humidity [6]. On the outer layer of surgical masks infectious virus could be recovered after 7 days [7].

One of the strategies for protecting against transmission is the use of personal protective equipment (PPE), including face masks and eye protection. During certain phases of the COVID-19 pandemic, face masks became sparsely available. The single use of PPE created a great demand, resulting in critical delivery delays of weeks and months. On the other hand, the extensive use of face masks and other protective items has led to a new form of massive waste generation. The disposal of huge amounts of used PPE components is an organizational challenge and a previously underestimated hazard for the environment [8,9]. Due to the high stability and rapid transmission of the virus, the shortage of PPE and the environmental pollution, an easy to use and sustainable disinfection method is needed that can make an important contribution to combating the pandemic and protecting the environment through the safe recycling of PPE.

Ultraviolet (UV) irradiation, vaporized hydrogen peroxide, moist heat, microwave-generated steam processing and liquid chemicals have all been reported to sterilize PPE [10,11], but each method has its disadvantages. Any kind of mask comprises a combination of various materials, each of which is differently sensitive to chemical or radiation treatments. For example, liquid treatments such as alcohols require drying time, may cause oxidation, e.g. at metal clamps, and lead to a loss of filtering performance. Some materials are sensitive to heat or

Abbreviations: BSL3, biosafety level 3; FFP3, filtering facepiece 3; FCS, fetal calf serum; PPE, personal protective equipment; VI, Virus input; PFU/mL, plaque forming units per ml.

* Corresponding author at: Diagnostic- and Research Center for Molecular Biomedicine, Institute of Pathology, Medical University of Graz, Neue Stiftingtalstraße 6, 8010, Graz, Austria.
E-mail address: kurt.zatloukal@medunigraz.at (K. Zatloukal).

https://doi.org/10.1016/j.nbt.2021.10.001
Received 6 August 2021; Received in revised form 1 October 2021; Accepted 2 October 2021
Available online 6 October 2021

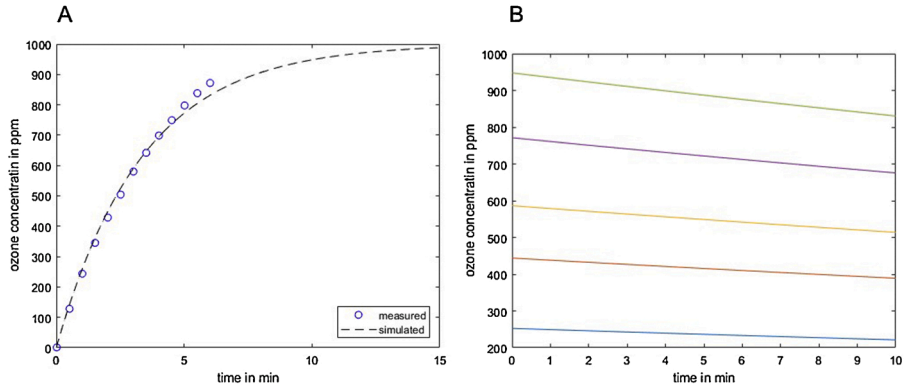

Fig. 1. A: Increase of ozone concentration (ppm) over time; B: Chemical ozone decomposition over time depending on initial concentration.

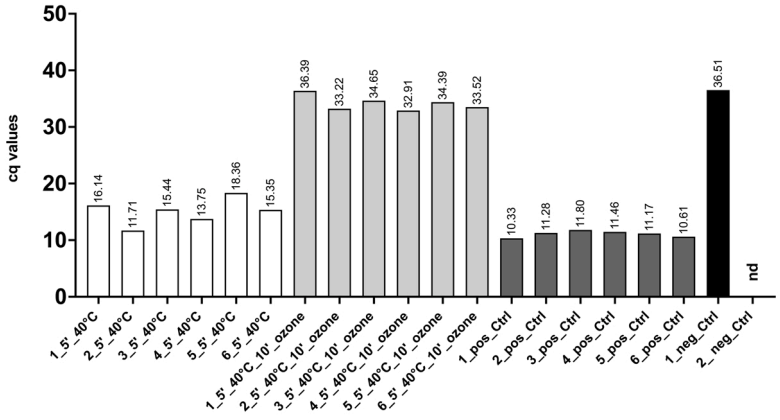

Fig. 2. Effect of ozone treatment on cotton masks. Heat-drying (5′ at 40 °C) alone or in combination with ozone treatment for 10 min, compared to positive controls (pos_Ctrl; cells infected with the same virus copy numbers as loaded on the masks). Cq values of 6 samples for each condition (5′_40 °C, 5′_40 °C_10′_ozone, pos_Ctrl) are shown. Non-infected cells (2 samples) served as negative controls (neg_Ctrl). Nd: not detectable.

chemicals, and UV light is unsuitable for materials with complex structures because areas shaded from the UV light will not be disinfected. Some masks also include electrostatically charged filter materials that may be adversely affected or even discharged by various treatments.

An alternative is the use of the strongly oxidizing gas ozone. Industrially, ozone is produced on a large-scale for water purification, paper and pulp processing, disinfection of plant and animal products as well as sterilization of medical supplies. It reacts with most elements of the periodic system except for noble metals, fluorine and the inert gases [12,13]. The antimicrobial activity of ozone has been reported for a broad range of bacterial targets on surfaces such as glass, plastic or steel. Its antiviral activity has been demonstrated for targets in enveloped and non-enveloped viruses, including the viral capsid, specific viral attachment epitopes and viral DNA/RNA [14–16]. Ozone disinfection of an N95 respirator has already been reported for *Pseudomonas aeruginosa,* which was selected as a test organism because of its spore-forming capacity and high resistance to disinfection processes. It was assumed that SARS-CoV-2 would likely be more susceptible to ozone disinfection than the other species tested. Exposure to ozone did not show significant changes in the filtering capacity of the N95 respirator after 10 cycles [17]. Ozone disinfection of artificially SARS-CoV-2-contaminated KF94 face masks, which are similar to N95 respirators, has been reported recently [18]. Moreover, the virus-inactivating activity of ozone was demonstrated for different metals, contaminated with a corona pseudovirus and HuCoV-229E, such as stainless steel, nickel and copper as well as glass [19]. Since ozone dosages for disinfection of different surfaces vary, a process is needed that is suitable for hard materials and PPE [20,21].

To address the need for safe and easy disinfection an experimental disinfection chamber has been developed (TDK Electronics GmbH & Co OG, Deutschlandsberg, Austria). The heart of the chamber is the patented cold plasma generator (CeraPlas™ element), the function of which is based on piezoelectric direct discharge (PDD) [22]. This converts a low periodic input signal into a high output voltage via piezoelectric coupling effects and enables the ionization of the surrounding gas at atmospheric pressure and ambient temperature. The generator provides a high ionization rate and an efficient ozone generation rate. Advantages are the low energy consumption during the ignition of the cold plasma in air at atmospheric pressure, the low thermal load for test materials (below 50 °C) and the compact dimensions. In addition, ozone generation enables the elimination of unpleasant odours. Cold plasma applications have increased in a variety of different fields over the last decades, including the automotive industry [23], medical devices, biomedical applications, skin care and surface treatments [24]. A relatively new application of cold plasma is the field of virus inactivation

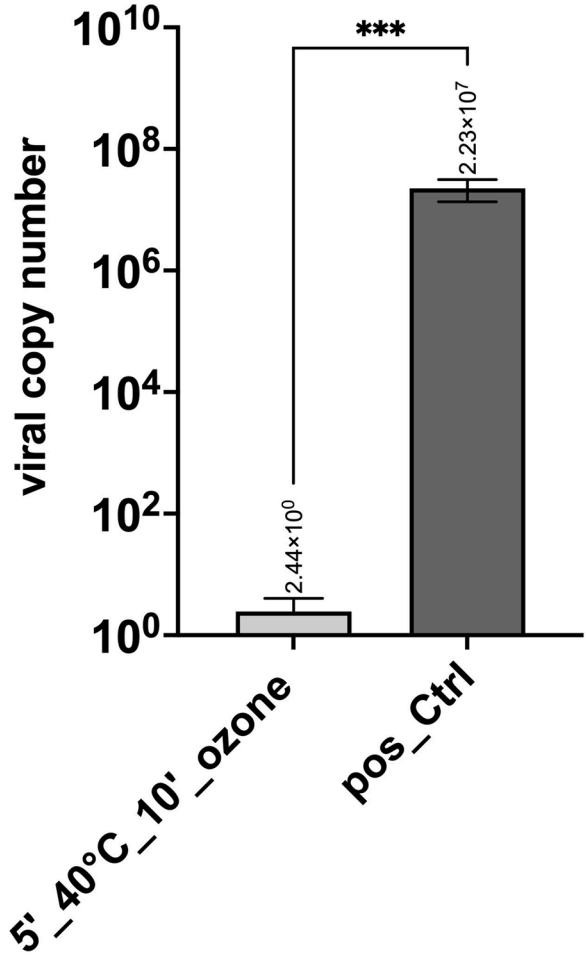

Fig. 3. Summary of data shown in Fig. 2 calculated for viral copy numbers based on an international certified SARS-CoV-2 RNA standard (ATCC VR-1986D™) that contains 4.73 × 10^3 genome copies per 1 µL. Heat-drying combined with ozone treatment led to a reduction in virus copy numbers in the range of log 7 in all six samples. Data is plotted in Log_{10} intervals. P value: 0.0001*** (t test).

research [25].

The aim of this study was to evaluate the disinfection capacity of ozone, generated within a newly developed disinfection chamber, against SARS-CoV-2 on cotton and FFP3 face masks as examples of porous materials, and on glass as an example of a non-porous material, to be used on a small scale, e.g. in homes, companies, offices, etc.

Material and methods

Ozone generation process for disinfection

The disinfection chamber developed (TDK Electronics GmbH & Co OG, Deutschlandsberg, Austria) is an experimental device to investigate the inactivation of SARS-CoV-2 on porous and non-porous surfaces. The prototype is an aluminium chamber with a nominal capacity of 1450 mL, containing a plasma generator and a microcontroller to regulate the disinfection process.

The virus-contaminated matrices undergoing the disinfection process are positioned on the metallic sample holder in the disinfection chamber, which is closed by a screw cap on the top (Supplementary Fig. S1). The plasma generator (CeraPlas™ element, Relyon Plasma GmbH, Regensburg, Germany) produces a cold plasma inside the disinfection chamber and ozone is generated as a side effect of the plasma generation. The ozone concentration was monitored before the experimental series to evaluate the reactive environment inside the disinfection chamber. During the experiments, no external air was supplied. After a time period of 10 or 60 min the disinfection chamber was opened in a laminar flow cabinet and was flushed with ambient air to terminate the disinfection process.

Cell culture

Vero CCL-81 cells (CCL-81™, ATCC, Manassas, VA, USA) were cultured in serum-free OptiPro medium (Thermo Fisher Scientific, Waltham, MA, USA) supplemented with 1% Penicillin-Streptomycin (Thermo Fisher Scientific) and 2% L-glutamine (Merck KGaA, Darmstadt, Germany) at 37 °C and 5% CO_2. Vero E6 cells (Biomedica, Vienna, Austria) were cultured in Minimal Eagle's Medium (MEM) (Thermo Fisher Scientific) supplemented with 5% fetal calf serum (FCS) (Thermo Fisher Scientific), 1% Penicillin-Streptomycin (Thermo Fisher Scientific) and 2% L-glutamine (Merck KGaA) at 37 °C and 5% CO_2.

Preparation of SARS-CoV-2 virus stock

All experimental procedures with SARS-CoV-2 were performed in a biosafety level (BSL)-3 laboratory at room temperature (RT, 22−24 °C) and 45 % relative humidity [26]. The experimental series were performed using a SARS-CoV-2 virus isolate (Human 2019-nCoV Isolate ex China Strain: BavPat1/2020) originated in the city of Wuhan (Hubei province, China). The virus was obtained under a licence agreement from the Charité University Hospital, Berlin, Germany (Institute of Virology, Prof. Drosten). Virus stocks were prepared by infecting VeroE6 cells with the virus isolate and incubating them at 37 °C and 5% CO_2 for 72 h. The cell culture supernatants were collected, centrifuged for 10 min at 3000 xg and sterile filtered using 0.2 µm syringe filters (Thermo Fisher Scientific, Waltham, USA). Adherent cells in cell culture flask were frozen with fresh medium, thawed again and scratched from the surface to release intracellular viral particles. Cell lysate samples were centrifuged for 10 min at 3000 xg to remove cell debris and sterile filtered using 0.2 µm syringe filters. Supernatants and cell lysates were pooled and stored at −80 °C. The virus titer was determined via the Spearman-Karber method [27]. In brief, VeroE6 cells were seeded in 48-well cell culture plates and infected with the serially diluted virus stock (6 wells for each dilution) for 1 h at 37 °C and 5% CO_2. After infection, cells were washed twice with MEM, then MEM supplemented with 2% FCS was added to each well and the cells were incubated at 37 °C and 5% CO_2 for 72 h. All wells were observed under the microscope to estimate the highest dilution at which all showed a cytopathic effect (CPE). The $TCID_{50}$ titer was calculated using the formula: $\log_{10}$ 50 % end point dilution = - (x_0 - d/2 + d $\sum$ r_i/n_i), where x_0 = $\log_{10}$ of the reciprocal of the highest dilution at which all wells showed CPE, d = $\log_{10}$ of the dilution factor, n_i = number of replicates used in each individual dilution, and r_i = number of positive wells (out of n_i). Summation was started at dilution x_0. The resulting $TCID_{50}$ titer per ml was multiplied by 0.7 to predict the number of PFU/mL [28].

Face mask preparation and ozone treatment

Cotton face masks (100 % cotton, white, Büro Handel GmbH, Villach, Austria) and FFP3 face masks (Blautex, Produktions- u Vertriebsges.m.b.H., Salzburg, Austria) were cut into circular pieces of 2 cm in diameter and were positioned in Petri dishes (60 mm diameter, Merck KGaA, Darmstadt, Germany). Each tested group consisted of 6 different pieces. The mask pieces were dried for 1 h at 40 °C in a BSL2 laboratory to reduce residual moisture prior to virus application. Thereafter, they were immediately taken to the BSL3 laboratory to be used for the virus neutralization assay. 50 µL of virus suspension (3.89E + 04 pfu/mL),

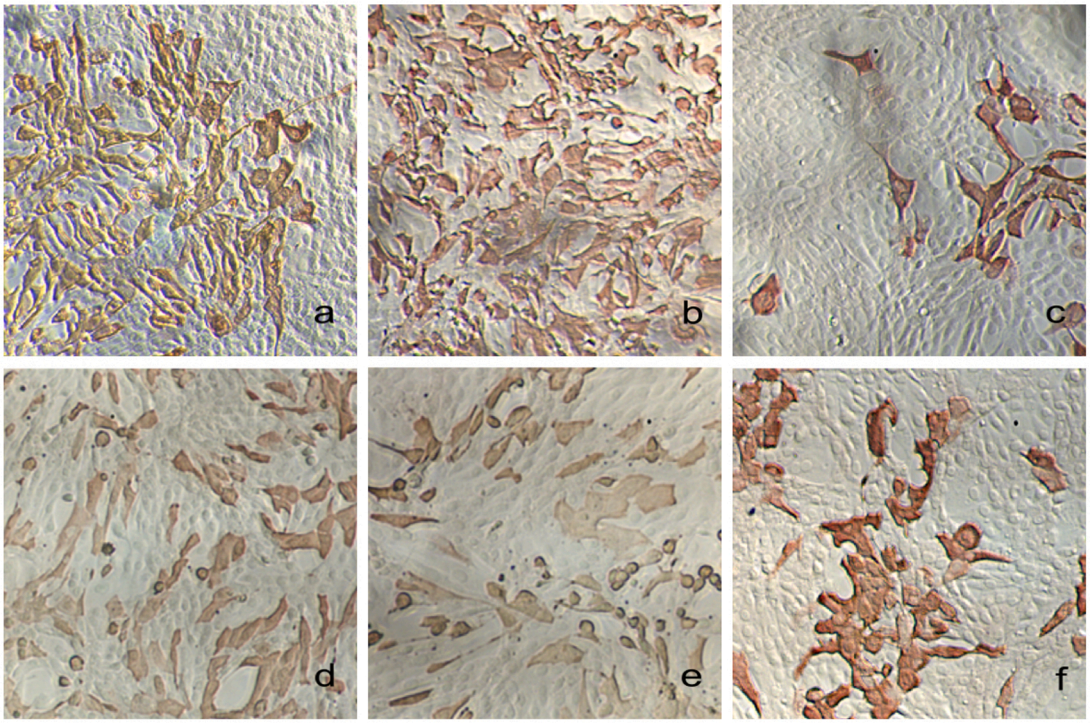

Fig. 4. Effect of heat-drying on recovery of infectious SARS-CoV-2 from cotton masks. CCL-81 cells were infected with virus recovered from cotton face masks after heat-drying for 5 min. Virus infected cells were stained red with SARS-CoV-2 (2019-nCoV) nucleocapsid antibody (Rabbit Mab; Sinobiological, China, Cat# 40,143-R019). The Ready-to-use detection system reagent EnVision™ + Dual Link System HRP (Agilent Dako, Cat# K5007) was used followed by incubation with AEC Substrate Chromogen (Agilent Dako, K346430-2). The reaction was stopped with PBS. An infection can be seen in all six samples (same experiment and sample labeling as shown as in Fig. 2). a: 1_5′_40 °C, b: 2_5′_40 °C, c: 3_5′_40 °C, d: 4_5′_40 °C, e: 5_5′_40 °C, f: 6_5′_40 °C. Magnification 100×.

buffered with 25 mM HEPES at pH 7.4, (Thermo Fisher Scientific) were spotted on and quickly absorbed by each mask piece. Subsequently, the samples were heat-dried for 5 min at 40 °C in an incubator and treated with ozone in the disinfection chamber for a total exposure time of 10 min. For the first 5 min, ozone was generated in the disinfection chamber until a concentration of 800 ppm was reached. This was then followed by 5 min additional exposure time in the closed chamber. Ozone decomposition to 750 ppm occurred over this time. Control mask pieces underwent the same procedure including heat-drying at 40 °C, but remained in the closed Petri dishes for the duration of the experiment and were not treated with ozone. For recovery of viral particles, the mask pieces were placed into 2 mL safe-lock tubes (Eppendorf Austria GmbH, Vienna, Austria) containing 1 mL serum-free OptiPro cell culture medium and were vortexed for 10 s. Samples were centrifuged for 10 min at 1500 xg and sterile filtered using 0.45 µm syringe filters (Merck KGaA, Darmstadt, Germany). 140 µL of each sample was collected to determine the recovered virus particles that served as virus input (VI) for the neutralization assay by viral RNA extraction and RT-qPCR (Supplementary Tables S1-S3).

Glass slide preparation for the SARS-CoV-2 stability test

Complementary to the procedure above for porous materials (face masks) the stability of SARS-CoV-2 was also tested on non-porous glass surfaces. Glass slides (LACTAN, Chemikalien und Laborgeräte Vertriebsgesellschaft m.b.H & Co KG, Graz, Austria) were cut to 2 × 2 cm and cleaned with 70 % ethanol. Each tested group consisted of 3 glass slides. The slides were pre-treated for 20 s with cold plasma, produced with a Piezo brush PZ2® (Relyon Plasma GmbH, Regensburg, Germany) to avoid droplet formation. Twenty µL of virus suspension (3.89E + 04 pfu/mL), buffered at pH 7.4 with 25 mM HEPES was spotted onto each plasma pre-treated glass slide. The slides were heat-dried at 40 °C for 10 min and then kept in closed Petri dishes at RT for 0, 1, 24 and 48 h, respectively. The dried virus suspensions on the slides were recovered after the different time periods by washing each slide with 500 µL of serum-free cell culture medium. Samples were collected to determine the VI before cell infection. Vero CCL-81 cells were infected with virus samples for 1 h at 37 °C and 5% CO_2. Cell culture supernatants were collected 48 h after each infection to determine viral copy numbers via viral RNA isolation and RT-qPCR (below).

Glass slide preparation for ozone treatment

Glass slides were cut to 2 × 2 cm, cleaned with 70 % ethanol and placed in 60 mm diameter Petri dishes. To avoid droplet formation on the surface, slides were pre-treated for 20 s with a Piezo brush PZ2® (Relyon Plasma GmbH, Regensburg, Germany). Each tested group consisted of 6 glass slides. Twenty µL of virus suspension (3.89E + 04 pfu/mL) buffered with 25 mM HEPES was spotted to each glass slide. All samples were heat-dried for 10 min at 40 °C. Glass slides were treated with ozone in the disinfection chamber for a total exposure time of 10 and 60 min. Ozone was initially generated for 5 min until a concentration of 800 ppm was reached, followed by 5 or 55 min exposure in the closed chamber, during which ozone decomposition to 750 ppm (5 min) or 400 ppm (55 min) occurred. Control samples were heat-dried at 40 °C and kept in closed Petri dishes without ozone treatment for the duration of the experiment. Slides were then washed with 500 µL of serum-free OptiPro cell culture medium for virus recovery. Samples were collected for determination of the VI and Vero CCL-81 cells were infected with the virus suspensions. Cell culture supernatants were

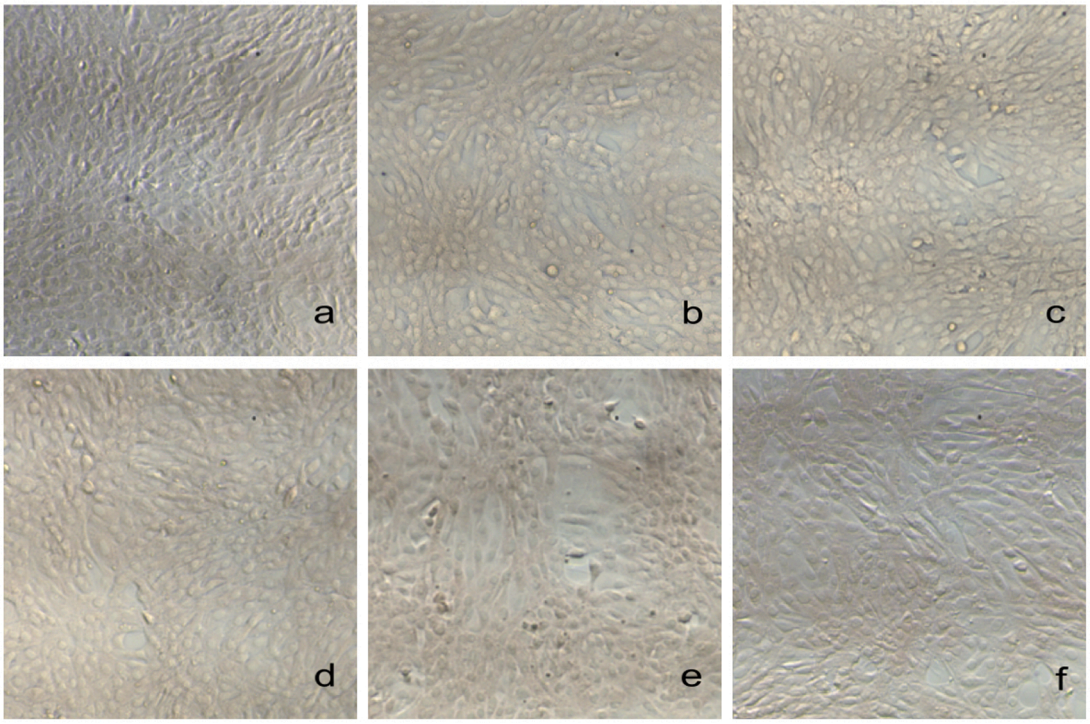

Fig. 5. Effect of heat-drying and ozone treatment on recovery of SARS-CoV-2 from cotton masks. CCL-81 cells were infected with virus recovered from cotton face masks after heat-drying for 5 min and ozone treatment. Virus infected cells were stained red with SARS-CoV-2 nucleocapsid antibody as in Fig. 4. No infection can be seen in all six samples (same experiment and sample labeling as shown in Fig. 2). a: 1_5′_40 °C_10′_ozone, b: 2_5′_40 °C_10′_ozone, c:3_5′_40 °C_10′_ozone, d: 4_5′_40 °C_10′_ozone, e: 5_5′_40 °C_10′_ozone, f: 6_5′_40 °C_10′_ozone. Magnification 100x.

collected 72 h after each infection to determine viral copy numbers via viral RNA isolation and RT-qPCR (below).

Infection assays

For infection assays 30,000 Vero CCL-81 cells per well were seeded into 48-well cell culture plates (Corning Incorporated, Kennebunk, ME, USA) 24 h prior to virus infection. The cells were infected with the virus recovered from the samples (VI) prepared as described above for 1 h at 37 °C and 5 % CO_2. For infection assay controls the same amount of virus suspension as applied onto the different matrices was mixed with serum-free OptiPro cell culture medium and was applied to the cells for infection. Non-infected cells served as negative controls. After infection the cells were washed twice with phosphate buffered saline (PBS) (Thermo Fisher Scientific). 440 µL serum-free cell culture medium was added to the cells and 140 µL supernatant of each well was collected subsequently to determine the timepoint 0 (t0) values. SARS-CoV-2 replicates rapidly in Vero CCL-81 cells and reaches peak titers between 48−72 h post infection [29]; thus incubation times of 48 or 72 h at 37 °C and 5% CO_2 were chosen. After the incubation period, 140 µL cell culture supernatant was removed from each well to determine the virus copy numbers at the timepoints (t48, t72) post infection via viral RNA extraction and RT-qPCR (below).

RNA isolation and quantitative, real-time PCR (RT-qPCR)

Viral RNA was isolated using the QIAamp® Viral RNA Mini Kit (Qiagen, GmbH, Hilden, Germany) according to the manufacturer's recommendations. RNA samples were eluted with 40 µL Milli-Q water and stored at −80 °C. RT-qPCR was performed using a Rotor-Gene Q thermal cycler (Qiagen) and the QuantiTect®Probe PCR Kit (Qiagen). Primers and probe sequences for the SARS-CoV-2 nucleocapsid N1 region were used as recommended by the Centers for Disease Control and Prevention (CDC) in February 2020 [30] and obtained from Eurofins Genomics (Ebersberg, Germany). Primer and probe sequences, PCR mastermix components and thermal profile are shown in Supplementary information, Tables 1–3.

Immunohistochemistry (IHC)

For the immunohistochemical detection of SARS-CoV-2 in infected cells, 48-well plates were fixed for 30 min with 4% neutral-buffered formalin and were washed 3 times with PBS. Plates were incubated with 0.1 % Triton X-100 (Merck KGaA) for 10 min, washed 3x with PBS and incubated for 30 min in 3% H_2O_2 (Merck KGaA) dissolved in methanol (Merck KGaA, Darmstadt, Germany). After a further PBS washing step, 100 µL of the primary antibody, SARS-CoV-2 (2019-nCoV) Nucleocapsid Antibody (Rabbit monoclonal antibody (Mab); Sinobiological, China, Cat# 40,143-R019) diluted 1:1000 in REAL Antibody Diluent (Agilent Dako, Carpinteria, CA, USA, Cat# S202230−3) was added to each well. The plates were washed 3 times with PBS after 1 h incubation at RT. The Ready-to-use detection system reagent EnVision™ + Dual Link System HRP (Agilent Dako, Cat# K5007) was added for 30 min, followed by washing with PBS 3 times. AEC Substrate Chromogen (Agilent Dako, K346430−2) was applied to each well and incubated for 3 min, and the reaction was stopped by adding PBS. Wells were washed again with PBS to remove reagent and fresh PBS was added to keep the wells humid. Images were taken by light microscope (Nikon, Eclipse, TS100; Nikon Europe BV, Amsterdam, Netherlands) equipped with a JENOPTIK GRYPHAX® camera (Breitschopf, Innsbruck, Austria). SARS-CoV-2 infected cells appear red after antibody staining.

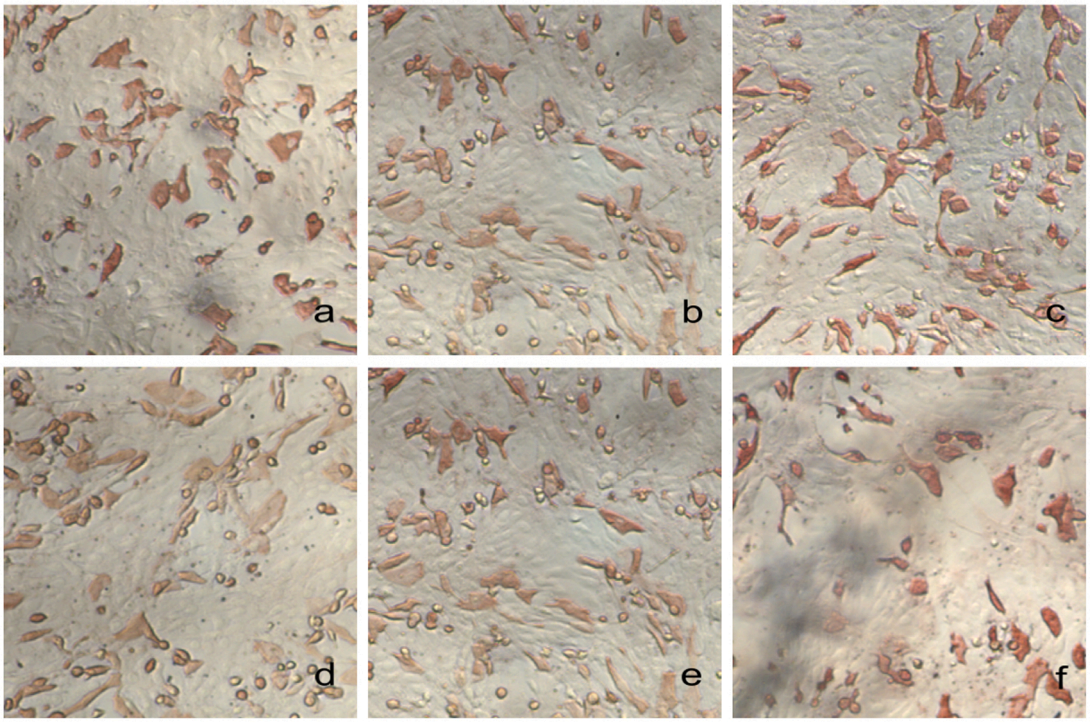

Fig. 6. Positive control for virus inactivation assay. CCL-81 cells were infected with same virus copy numbers as loaded on cotton face masks. Virus infected cells were stained red with SARS-CoV-2 nucleocapsid antibody as in Fig. 4. Infection can be seen in all six samples (same experiment and sample labeling as shown in Fig. 2). a: 1_pos_Ctrl, b: 2_pos_Ctrl, c: 3_pos_Ctrl, d: 4_pos_Ctrl, e: 5_pos_Ctrl, f: 6_pos_Ctrl. Magnification 100x.

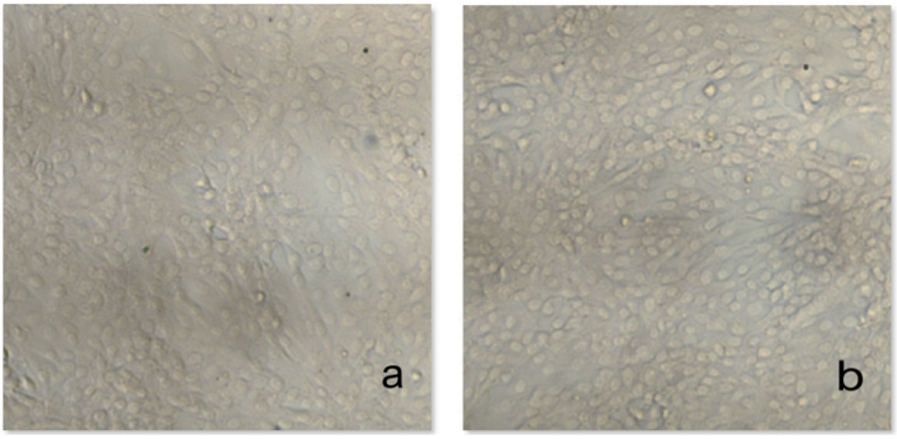

Fig. 7. Negative control for virus inactivation assay. Non-infected Vero CCL-81 cells were stained with SARS-CoV-2 nucleocapsid antibody as in Fig. 4. No virus can be seen in either sample (same experiment as shown in Fig.2). Magnification 150x.

Data analysis

Data analysis, copy number calculations, statistics and graphical presentations were performed with GraphPad Prism 9. Statistical differences between groups were determined using *t*-test and One-way ANOVA corrected for multiple comparisons. Symbols are: ns = $P > 0.05$; * = $P \leq 0.05$; ** = $P \leq 0.01$; *** = $P \leq 0.001$; **** = $P \leq 0.0001$.

To calculate viral copy numbers based on the RT-qPCR cq-values a calibration curve (Supplementary Figure S3) based on a certified RNA standard (ATCC VR-1986D™) was used. This standard contains 4.73×10^3 genome copies per 1 µL. Viral copy numbers of VI, t48 and t72 were calculated using the resulting equation $y = 1.422x + 35.079$.

Results

Ozone generation for disinfection

Ozone was generated by the cold plasma source inside the

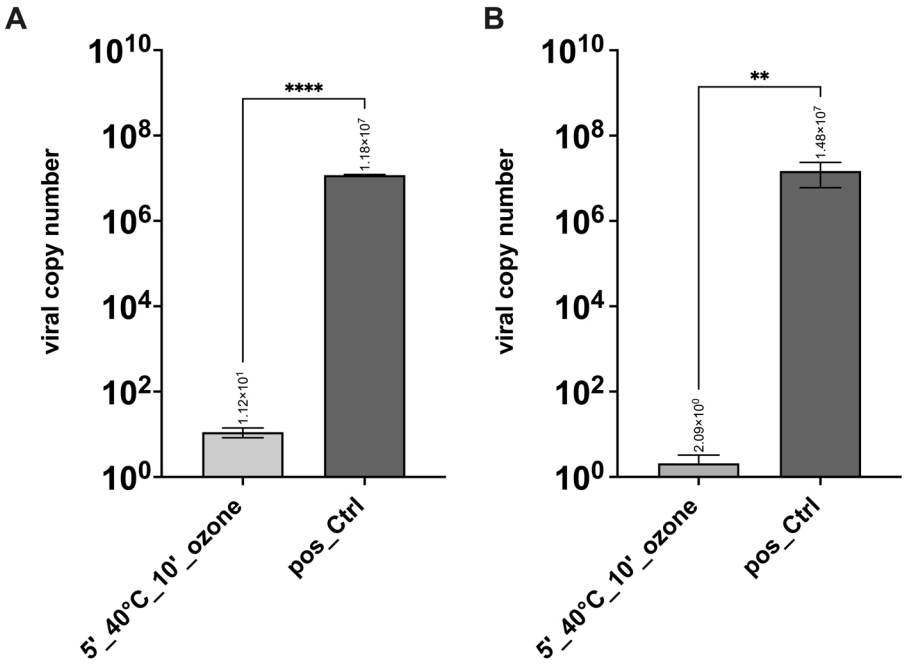

Fig. 8. A: Effect of ozone treatment on FFP3 masks on recovery of infectious SARS-CoV-2. Results are shown from two independent experimental series with 6 samples per experimental condition, each. A: Experimental series 1 showing virus copy numbers from heat-dried (5′ at 40 °C) and 10′ ozone-treated samples compared to positive control (cells infected with same copy numbers as loaded on masks). P value: <0.0001**** B: Experimental series 2 showing virus copy numbers from heat-dried (5′ at 40 °C) and 10′ ozone-treated samples compared to positive control (cells infected with same copy numbers as loaded on masks). Data is plotted in Log_{10} intervals. P value: 0.0021** (t test).

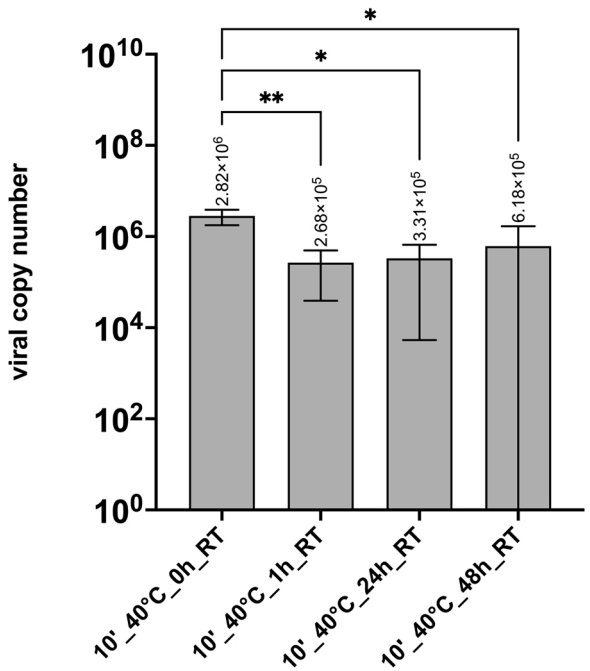

Fig. 9. Stability and infectivity of SARS-CoV-2 on glass slides after drying at 40 °C for 10 min and storage of up to 48 h at RT. Viral copy numbers were calculated using a certified reference standard. Infectious virus was determined by infecting Vero CCL-81 cells with virus recovered from glass surface at different time points. Each group consisted of biological triplicates. Data is plotted in Log_{10} intervals. P value: 0.0106* (One-way ANOVA).

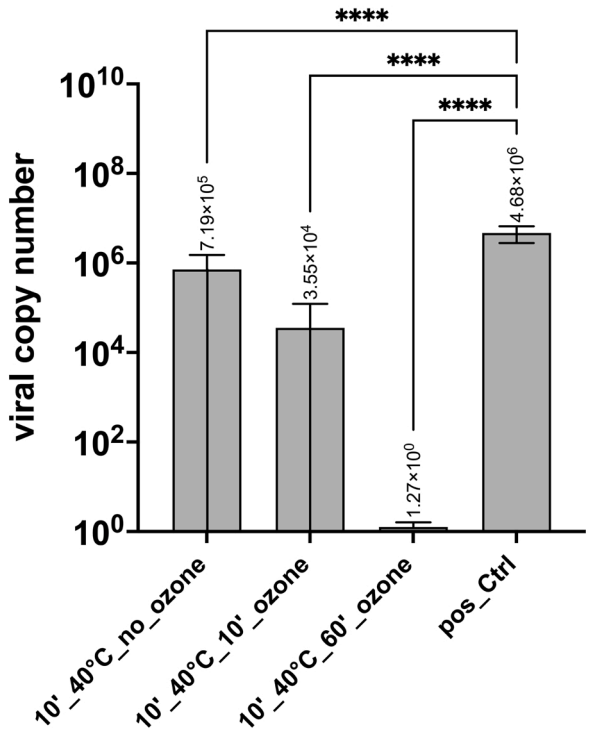

Fig. 10. SARS-CoV-2 inactivation on glass surface by ozone. Virus was recovered from glass slides after drying (10′ at 40 °C) and ozone treatment (either 10′ or 60′) and used for infection of Vero CCL-81 cells. Cells infected with the same virus copy number as loaded on the slides served as positive controls (pos_Ctrl). After drying and 60 min ozone treatment a reduction of infectious virus by a factor of > log 6 was obtained. All groups consisted of 6 replicates, each. Data is plotted in Log_{10} intervals. P value: <0.0001**** (One-way ANOVA).

disinfection chamber. The ozone-based disinfection process is divided in two phases: generation (phase 1) and chemical decomposition (phase 2). The disinfection process of the virus-contaminated surfaces begins in phase 1. The exponential increase of ozone concentration inside the disinfection chamber over time is shown in Fig. 1A. After the cold plasma source is terminated, the disinfection chamber remains closed and the chemical decomposition phase begun [31]. Ozone concentration inside the chamber decreases in the sealed container during the chemical decomposition time as shown in Fig. 1B.

In this study an ozone generation time of 5 min was performed for all surfaces tested, resulting in a maximal concentration of 800 ppm inside the chamber. The additional exposure of 5 min for FFP3 and cotton face masks led to a decomposition of ozone to 750 ppm. The 55 min additional exposure for the glass surfaces resulted in decomposition to 400 ppm (Supplementary Information, Fig. S2). After phase 2 the disinfection test chamber was opened in a laminar flow cabinet and flushed with ambient air, which terminates the disinfection process.

SARS-CoV-2 inactivation by ozone treatment of cotton face masks

Cotton masks loaded with SARS-CoV-2 showed that heat-drying for 5 min in combination with ozone treatment of 10 min (Fig. 2; 5′_40 °C_10′_ozone) led to virus reduction by a factor of $>8.99 \times 10^6$ in all 6 samples compared to the positive controls. In contrast, heat-drying without ozone treatment (Fig. 2; 5′_40 °C) led only to minor inactivation of up to log 1 in the tested samples and the virus particles remained infectious, as indicated by the low cq values reflecting the high number of virus particles released into the cell culture medium during 72 h post-infection. As positive controls, cells were infected with the same virus copy numbers as loaded on the masks, with non-infected cells as negative controls. The amount of virus recovered from the mask pieces after ozone treatment and from control masks, which was the virus input (VI) for cell infection (VI is shown in the Supplementary Fig. S4). Recovery of virus particles was similar for each tested group, underlining that the cells were infected with approximately the same number. Moreover, virus particles were measured at t0 (after infection and washing the cells with PBS and addition of fresh cell culture medium, Supplementary Fig. S5) to obtain a baseline value, and the increase in measured virus particles after the cultivation period (e.g. t72 – t0) was used to calculate virus replication. In order to calculate virus copy numbers from cq values obtained by RT-qPCR, a standard curve using a certified SARS-CoV-2 RNA standard was generated (Supplementary Figure S3). Results demonstrate that heat-drying in combination with ozone treatment yielded more than log 7 inactivation of SARS-CoV-2 compared to the positive controls (infected cells) as shown in Fig. 3.

The effect of ozone-treatment of cotton masks on virus inactivation was also analyzed by using an antibody to the SARS-CoV-2 nucleocapsid protein as independent read-out (Figs. 4–6). SARS-CoV-2 infected cells appear red after IHC staining. Stained cell culture plates demonstrate that virus recovered from heat-dried masks without ozone treatment was still infectious (Fig. 4). The absence of SARS-CoV-2 infected cells is confirmed by antibody staining in all 6 wells that were incubated with virus recovered from masks dried at 40 °C for 5 min and then treated with ozone for 10 min (Fig. 5). Cells infected with the same virus copy number as applied to the mask pieces were used as positive controls. In this case infection can be seen in all 6 wells (Fig. 6). In Fig. 7, non-infected cells stained with SARS-CoV-2 antibody serving as negative control are shown. In both samples no virus infection can be seen.

SARS-CoV-2 inactivation by ozone treatment of FFP3 masks

In line with the results for the cotton masks, the combination of heat-drying and ozone treatment of FFP3 masks resulted in virus inactivation by a factor of log 6 in all tested samples. Two independent experimental series were carried out using 6 mask pieces for each testing condition as described above. Viral copy numbers for heat-dried and ozone-treated samples (Fig. 8; 5′_40 °C_10′_ozone) were compared to positive controls (Fig. 8; pos_Ctrl). A virus inactivation of > log 6 was achieved in both experimental series.

SARS-CoV-2 stability and inactivation on glass surface

In order to test the stability of SARS-CoV-2 on non-porous surfaces, glass slides were loaded with virus and recovery of infectious virus was tested after different time periods. Immediately after loading and heat-drying at 40 °C, a mean viral copy number of 2.82×10^6 of infectious SARS-CoV-2 virus was recovered (Fig. 9). After 1 h at RT, detectable infectious virus was reduced to 2.68×10^5. Interestingly, the mean viral copy number did not decrease further after 24 h or 48 h at RT. Thus, SARS-CoV-2 is stable and infectious on non-porous surfaces for at least 48 h at RT.

SARS-CoV-2 inactivation by ozone treatment of glass surface

Glass slides were loaded with SARS-CoV-2 suspension and Vero CCL-81 cells were infected with recovered virus to test virus inactivation. After drying at 40 °C for 10 min, infectious virus was reduced by a factor of log 1 compared to the positive control, while drying and ozone treatment for 10 min led to a further reduction by a factor of log 1. Drying and ozone treatment for 1 h led to virus inactivation by a factor of > log 6 (Fig. 10). The virus neutralizing activity was confirmed by antibody staining which showed no infected cells in wells of the slides dried and ozone-treated for 1 h (data not shown).

Discussion

The wearing of face masks and other PPE is an important measure to protect from SARS-CoV-2 infection. Disadvantages of these single-use products are supply chain and production difficulties due to the enormous demand during the pandemic. This has led to shortages in production capacity particularly for masks with higher protection levels, such as FFP2 and FFP3, which are needed for healthcare professionals, and were also required for the general population in several countries in the SARS-CoV-2 wave in spring 2021. As a further consequence, immense amounts of waste were generated which became a major environmental issue. Safe and sustainable recycling methods could be an alternative to discarding products after single use.

This work describes a highly efficient disinfection process for SARS-CoV-2 that can be applied to porous and non-porous surfaces, demonstrated with different types of masks as well as glass slides, to exemplify a non-porous surface found on a variety of personal items such as mobile phones, tablets, watches or glasses. The combination of heat-drying and ozone treatment resulted in a virus reduction of more than log 6 for cotton and FFP3 masks as well as for glass slides. According to the guideline of the German Association for the control of virus diseases (DVV) and the Robert Koch Institute (RKI) a reduction of at least log 4 is required for virus-inactivating disinfectants [32]. Hence, the combination of drying and ozone treatment appears to represent a suitable method for decontamination of various surfaces. However, different properties of surfaces for stabilization and inactivation of virus have to be considered and tested for specific applications. For example, Zucker and co-workers [19] demonstrated different surface tensions of virus-containing droplets on different metal surfaces and glass, which was mirrored by different virus-inactivating activities of ozone. Whether the drying-step included in our experiments overcomes and or mitigates this effect has to be determined.

The virus concentration used in this work for the application on the different materials was 3.89×10^4 PFU/mL, which corresponds to a mean cq value of 18.5 for positive controls after sample treatment and recovery as shown for the cotton face mask (Supplementary Figure S4). When calculated for viral copy numbers based on a reference standard this corresponds to 1.16×10^5 viral copies. Viral load from a single

cough from a person with a high viral load in respiratory fluid may generate $>10^5$ viral copies [33]. The viral load used for sample loading in this work therefore corresponds to amounts that could be transmitted by contagious individuals.

The different ozone treatment times of materials described in this work can be explained by their structures. Cotton masks are not intended for medical use and are not certified. However, they prevent the spread of potentially contagious droplets. This type of mask is reusable after washing but disinfection with ozone would save time and be less damaging to the fabric compared to daily washing. FFP3 masks provide the most effective protection for users with a minimum filtration percentage of 99 % for very fine particles [34]. According to the manufacturers, FFP3 masks have a limited lifespan of a few hours, after which their filtration efficiency can no longer be guaranteed and they should be discarded. Cotton fabrics and layered FFP3 masks have much larger surfaces than glass slides. These masks absorb virus suspensions quickly leading to a large surface distribution in the materials. As a result, the contact surface for ozone increases and the samples are disinfected within short time periods.

Liquids on glass surfaces form droplets due to the non-porosity of the surface. Preliminary experiments showed that if treated with ozone, virus particles in droplets cannot be inactivated because of the surface tension. To overcome this effect, test glass slides were pre-treated with cold plasma. This surface treatment was chosen because a liquid film represents a more realistic setting than a large droplet. The surface energy of inorganic materials like glass is increased by plasma treatment. Without treatment, glass has a surface energy of 47 mN/m. After treatment with a piezo brush PZ2®, the surface energy increased to >67 mN/m [35]. If the surface energy of the glass slide is the same or greater than that of the liquid, the liquid will spread on the surface resulting in virus contamination resembling that of aerosols. This fact makes the wetting of non-porous surfaces possible and allows the distribution of the virus suspension on the glass surfaces for testing of disinfection procedures [36]. The resulting liquid film can then be heat-dried in 10 min. Disinfection with ozone for 10 min is effective for some, but not all, treated samples. This is most likely due to the non-uniform drying of the liquid film. However, after an ozone treatment of 60 min an efficient disinfection (>log 6 reduction of infectious virus) for all glass slides treated with a combination of heat and ozone can be achieved (Fig. 10).

In contrast to other disinfection methods, gaseous ozone has many advantages. Its high reactivity makes it useful as a disinfectant for bacterial and viral contaminations which has been described in detail [14–16]. Ozone penetrates complex objects such as layered face masks from all sides and reaches every surface of the sample that cannot be achieved with e.g. alcohol or UV light. It is thermodynamically unstable and its breakdown product, oxygen, is environmentally harmless. However, when inhaled, ozone can cause adverse respiratory effects, such as shortness of breath, chest pain, wheezing, coughing and airway inflammation, While long term exposure has been linked to the development of asthma and may be associated with lung cancer [14,37–39]. Consequently, the direct opening of the disinfection chamber is only possible under laboratory conditions and in a laminar flow cabinet. To guarantee maximal safety for the future use of ozone-producing disinfection devices outside of the laboratory, the installation of a catalyst for the active chemical decomposition of ozone before opening the device is easily implemented. One commonly used catalyst is manganese oxide and other options are platinum group metals, less widely used due to their high cost [13,40].

Conclusion

The results of this work present a highly efficient combined heat-drying and ozone treatment process that is suitable for the disinfection of various porous and non-porous SARS-CoV-2 contaminated surfaces. A reduction of more than log 6 for SARS-CoV-2 was demonstrated for cotton and FFP3 masks and for glass slides. The method could help to overcome delivery difficulties of face masks and reduce waste caused by single-use PPE. The disinfection of other personal items of daily life is also within scope as well as industrial applications.

Funding

This work was funded by TDK Electronics GmbH & Co OG.

Declaration of Competing Interest

RelyOn Plasma is a subsidiary of the TDK company and provided the apparatus for the study. The co-authors M. Puff and A. Melischnig are employees of TDK Electronics and co-inventors of the technology, which is owned by TDK-Electronics. They declare no conflict of interest in relation to this study.

Acknowledgments

We thank the members of the BSL3 laboratory team for their scientific and logistical support. Special thanks to Julia Rieger for assistance in the BSL3 laboratory, and to Daniel Habich, Daniela Pabst and Stephanie Freydl for their help in RNA isolation and cell culture. Thanks to Penelope Kungl and Thomas Koidl for help in proof reading of the document.

Appendix A. Supplementary data

Supplementary material related to this article can be found, in the online version, at doi:https://doi.org/10.1016/j.nbt.2021.10.001.

References

[1] Harrison AG, Lin T, Wang P. Mechanisms of SARS-CoV-2 transmission and pathogenesis. Trends Immunol 2020;41:1100–15. https://doi.org/10.1016/j.it.2020.10.004.
[2] Ye G, Lin H, Chen S, Wang S, Zeng Z, Wang W, et al. Environmental contamination of SARS-CoV-2 in healthcare premises. J Infect 2020;81:e1–5. https://doi.org/10.1016/j.jinf.2020.04.034.
[3] Ding S, Liang TJ. Is SARS-CoV-2 Also an Enteric Pathogen With Potential Fecal–Oral Transmission? A COVID-19 Virological and Clinical Review. Gastroenterology 2020;159:53–61. https://doi.org/10.1053/j.gastro.2020.04.052.
[4] Tian Y, Rong L, Nian W, He Y. Review article: gastrointestinal features in COVID-19 and the possibility of faecal transmission. Aliment Pharmacol Ther 2020;51:843–51. https://doi.org/10.1111/apt.15731.
[5] Riddell S, Goldie S, Hill A, Eagles D, Drew TW. The effect of temperature on persistence of SARS-CoV-2 on common surfaces. Virol J 2020;17:1–7. https://doi.org/10.1186/s12985-020-01418-7.
[6] Chan KH, Peiris JSM, Lam SY, Poon LLM, Yuen KY, Seto WH. The effects of temperature and relative humidity on the viability of the SARS coronavirus. Adv Virol 2011;2011. https://doi.org/10.1155/2011/734690.
[7] Chin AWH, Poon LLM. Stability of SARS-CoV-2 in different environmental conditions – authors' reply. The Lancet Microbe 2020;1:e146. https://doi.org/10.1016/S2666-5247(20)30095-1.
[8] Torres FG, De-la-Torre GE. Face mask waste generation and management during the COVID-19 pandemic: an overview and the Peruvian case. Sci Total Environ 2021;786:147628. https://doi.org/10.1016/j.scitotenv.2021.147628.
[9] Chowdhury H, Chowdhury T, Sait SM. Estimating marine plastic pollution from COVID-19 face masks in coastal regions. Mar Pollut Bull 2021;168:112419. https://doi.org/10.1016/j.marpolbul.2021.112419.
[10] Schumm MA, Hadaya JE, Mody N, Myers BA, Maggard-Gibbons M. Filtering facepiece respirator (N95 respirator) reprocessing. JAMA 2021. https://doi.org/10.1001/jama.2021.2531.
[11] Ludwig-Begall LF, Wielick C, Dams L, Nauwynck H, Demeuldre P-F, Napp A, et al. The use of germicidal ultraviolet light, vaporized hydrogen peroxide and dry heat to decontaminate face masks and filtering respirators contaminated with a SARS-CoV-2 surrogate virus. J Hosp Infect 2020;106:577–84. https://doi.org/10.1016/j.jhin.2020.08.025.
[12] Oyama ST. Chemical and catalytic properties of ozone. Catal Rev - Sci Eng 2000;42:279–322. https://doi.org/10.1081/CR-100100263.
[13] Batakliev T, Georgiev V, Anachkov M, Rakovsky S, Rakovsky S. Ozone decomposition. Interdiscip Toxicol 2014;7:47–59. https://doi.org/10.2478/intox-2014-0008.
[14] Greene AK, Güzel-Seydim ZB, Seydim AC. Properties of ozone. Ozone Food Process 2012:2.

[15] Torrey J, von Gunten U, Kohn T. Differences in viral disinfection mechanisms as revealed by quantitative transfection of echovirus 11 genomes. Appl Environ Microbiol 2019;85. https://doi.org/10.1128/AEM.00961-19.
[16] Murray BK, Ohmine S, Tomer DP, Jensen KJ, Johnson FB, Kirsi JJ, et al. Virion disruption by ozone-mediated reactive oxygen species. J Virol Methods 2008;153:74–7. https://doi.org/10.1016/j.jviromet.2008.06.004.
[17] Manning EP, Stephens MD, Patel S, Dufresne S, Silver B, Gerbarg P, et al. Disinfection of N95 respirators with ozone. MedRxiv 2020. https://doi.org/10.1101/2020.05.28.20097402.
[18] Lee J, Bong C, Lim W, Bae PK, Abafogi AT, Baek SH, et al. Fast and easy disinfection of coronavirus-contaminated face masks using ozone gas produced by a dielectric barrier discharge plasma generator. Environ Sci Technol Lett 2021;8:339–44. https://doi.org/10.1021/acs.estlett.1c00089.
[19] Zucker I, Lester Y, Alter J, Werbner M, Yecheskel Y, Gal-Tanamy M, et al. Pseudoviruses for the assessment of coronavirus disinfection by ozone. Environ Chem Lett 2021;19:1779–85. https://doi.org/10.1007/s10311-020-01160-0.
[20] Clavo B, Córdoba-Lanús E, Rodríguez-Esparragón F, Cazorla-Rivero SE, García-Pérez O, Piñero JE, et al. Effects of ozone treatment on personal protective equipment contaminated with SARS-CoV-2. Antioxidants 2020;9:1222. https://doi.org/10.3390/antiox9121222.
[21] Blanco A, Ojembarrena F de B, Clavo B, Negro C. Ozone potential to fight against SAR-COV-2 pandemic: facts and research needs. Environ Sci Pollut Res 2021;28:16517–31. https://doi.org/10.1007/s11356-020-12036-9.
[22] Nettesheim S, Korzec D, Burger D, Kügerl G, Puff M, Hoppenthaller F. Device for creating a plasma and handheld apparatus using this device. 2014. p. 19. https://data.epo.org/gpi/EP2948991A1-DEVICE-FOR-CREATING-A-PLASMA-AND-HANDHELD-APPARATUS-USING-THIS-DEVICE.
[23] Krasa H, Schriefl MA, Kupper M, Melischnig A, Bergmann A. Aerosol charging with a piezoelectric plasma generator. Plasma 2021;4:377–88. https://doi.org/10.3390/plasma4030027.
[24] Nettesheim S, Burger D, Szulc M, Falk W, Guido P. Effect of piezoelectric direct discharge plasma on microorganisms. Relyon Plasma 2015:20–3. https://www.relyon-plasma.com/effect-of-piezoelectric-direct-discharge-plasma-on-microorganisms/?lang=en.
[25] Filipić A, Gutierrez-Aguirre I, Primc G, Mozetič M, Cold Plasma Dobnik D. A new hope in the field of virus inactivation. Trends Biotechnol 2020;38:1278–91. https://doi.org/10.1016/j.tibtech.2020.04.003.
[26] Loibner M, Langner C, Regitnig P, Gorkiewicz G, Zatloukal K. Biosafety requirements for autopsies of patients with COVID-19: example of a BSL-3 autopsy facility designed for highly pathogenic agents. Pathobiology 2021;88:37–45. https://doi.org/10.1159/000513438.
[27] Ramakrishnan MA. Determination of 50% endpoint titer using a simple formula. World J Virol 2016;5:85. https://doi.org/10.5501/wjv.v5.i2.85.
[28] ATCC. Is it possible to determine from the TCID[50] how many plaque forming units to expect? n.d. https://www.atcc.org/support/technical-support/faqs/converting-tcid-50-to-plaque-forming-units-pfu.
[29] Harcourt J, Tamin A, Lu X, Kamili S, Sakthivel Sk, Murray J, et al. Severe acute respiratory syndrome coronavirus 2 from patient with coronavirus disease. United States. Emerg Infect Dis 2020;26:1266–73. https://doi.org/10.3201/EID2606.200516.
[30] CDC. Research use only 2019-Novel coronavirus (2019-nCoV) real-time RT-PCR primers and probes. 2020. https://www.cdc.gov/coronavirus/2019-ncov/lab/rt-pcr-panel-primer-probes.html.
[31] McClurkin JD, Maier DE, Ileleji KE. Half-life time of ozone as a function of air movement and conditions in a sealed container. J Stored Prod Res 2013;55:41–7. https://doi.org/10.1016/j.jspr.2013.07.006.
[32] Rabenau HF, Schwebke I, Blümel J, Eggers M, Glebe D, Rapp I, et al. Guideline for testing chemical disinfectants regarding their virucidal activity within the field of human medicine. Bundesgesundheitsblatt - Gesundheitsforsch - Gesundheitsschutz 2020;63:645–55. https://doi.org/10.1007/s00103-020-03115-w.
[33] Wang Y, Xu G, Huang Y-W. Modeling the load of SARS-CoV-2 virus in human expelled particles during coughing and speaking. PLoS One 2020;15:e0241539. https://doi.org/10.1371/journal.pone.0241539.
[34] Li KKW, Joussen AM, Kwan JKC. Steel DHW. FFP3, FFP2, N95, surgical masks and respirators: what should we be wearing for ophthalmic surgery in the COVID-19 pandemic? Graefes Arch Clin Exp Ophthalmol 2020;258:1587–9. https://doi.org/10.1007/s00417-020-04751-3.
[35] Nettesheim S. Inorganic materials. Relyon Plasma GmbH n.d. https://www.relyon-plasma.com/wp-content/uploads/2016/09/technical-notes-activation-capacity-of-atmospheric-plasma-systems.pdf.
[36] Nettesheim S. Evaluating the activation capacity of atmospheric plasma systems. 2016. https://www.relyon-plasma.com/wp-content/uploads/2016/09/technical-notes-activation-capacity-of-atmospheric-plasma-systems.pdf.
[37] Nuvolone D, Petri D, Voller F. The effects of ozone on human health. Environ Sci Pollut Res 2018;25:8074–88. https://doi.org/10.1007/s11356-017-9239-3.
[38] Koman PD, Mancuso P. Ozone exposure, cardiopulmonary health, and obesity: a substantive review. Chem Res Toxicol 2017;30:1384–95. https://doi.org/10.1021/acs.chemrestox.7b00077.
[39] Filippidou E, Koukouliata A. Ozone effects on the respiratory system. Prog Heal Sci 2011;1:144–55.
[40] Dhandapani B, Oyama ST. Gas phase ozone decomposition catalysts. Appl Catal B Environ 1997;11:129–66.